

Modern Physics Letters A
© World Scientific Publishing Company

PRESSURE OF DEGENERATE AND RELATIVISTIC ELECTRONS IN A SUPERHIGH MAGNETIC FIELD

ZHI FU, GAO

1. *Xinjiang Astronomical Observatory, CAS, 150, Science 1-Street, Urumqi, Xinjiang, 830011, China. zhifu_gao@xao.ac.cn*
2. *Key Laboratory of Radio Astronomy, CAS, Nanjing, Jiangshu, 210008, China*

NA, WANG

Xinjiang Astronomical Observatory, CAS, 150, Science 1-Street, Urumqi Xinjiang, 830011, China

QIU HE, PENG

School of Astronomy and Space Science, Nanjing University, 22, Hankou Road, Nanjing, Jiangshu, 210093, China

XIANG DONG, LI

School of Astronomy and Space Science, Nanjing University, 22, Hankou Road, Nanjing, Jiangshu, 210093, China

YUAN JIE, DU

National Space Science Center, CAS, 1-Nanertiao, Zhongguancun, Haidian District, Beijing, 100190, China

Received (Day Month Year)

Revised (Day Month Year)

Based on our previous work, we deduce a general formula for pressure of degenerate and relativistic electrons, P_e , which is suitable for superhigh magnetic fields, discuss the quantization of Landau levels of electrons, and consider the quantum electrodynamic(QED) effects on the equations of states (EOSs) for different matter systems. The main conclusions are as follows: P_e is related to the magnetic field B , matter density ρ , and electron fraction Y_e ; the stronger the magnetic field, the higher the electron pressure becomes; the high electron pressure could be caused by high Fermi energy of electrons in a superhigh magnetic field; compared with a common radio pulsar, a magnetar could be a more compact oblate spheroid-like deformed neutron star due to the anisotropic total pressure; and an increase in the maximum mass of a magnetar is expected because of the positive contribution of the magnetic field energy to the EOS of the star.

Keywords: Landau levels; Superhigh magnetic fields; Fermi surface.

PACS: 71.70.Di; 97.0.L.d; 71.18.+y.

1. Introduction

Thompson and Duncan (1996) predicted that superhigh magnetic fields could exist in the interiors of magnetars, which are powered by extremely strong magnetic fields, $B \sim 10^{14}$ to 10^{15} G (see Ref. 1). The majority of magnetars are classified into two populations historically: the soft gamma-ray repeaters (SGRs), and the anomalous X-ray pulsars (AXPs). Pulsars have been recognized to be normal neutron stars (NSs), but sometimes have been argued to be quark stars (e.g., see Ref. 2, 3, 4).

It is universally accepted that 3P_2 anisotropic neutron superfluid could exist in the interior of a neutron star (NS). If the superhigh magnetic fields of magnetars originate from the magnetic fields induced by the ferromagnetic moments of the 3P_2 Cooper pairs of the anisotropic neutron superfluid at a moderate to lower temperatures ($T \ll 2.87 \times 10^8$ K, the critical temperature of the 3P_2 neutron superfluid) and high nuclear density ($\sim 0.5\rho_0 < \rho < 2.0\rho_0$), then the maximum magnetic field strength for the heaviest magnetar may be estimated to be $(3.0 \sim 4.0) \times 10^{15}$ G, according to our model (see Ref. 5, 6).

For completely degenerate ($T \rightarrow 0$, i.e., $\mu/kT \rightarrow \infty$, μ is the chemical potential of species i , also called the Fermi energy, $E_F(i)$) and relativistic electrons in equilibrium, the distribution function $f(E_e)$ can be expressed as

$$f(E_e) = \frac{1}{\text{Exp}[(E_e - \mu_e)/kT] + 1} , \quad (1)$$

where the sign + refers to Fermi-Dirac statistics, k represents Boltzmann's constant; and μ_e is the electron chemical potential; when $E_e \leq E_F(e)$, $f(E_e) = 1$; when $E_e > E_F(e)$, $f(E_e) = 0$. The electron Fermi energy $E_F(e)$ has the simple form

$$E_F^2(e) = p_F^2(e)c^2 + m_e^2c^4 , \quad (2)$$

with $p_F(e)$ being the electron Fermi momentum.

In the interior of a NS, when B is too weak to be taken into consideration, $p_F(e)$, is mainly determined by matter density ρ and the electron fraction Y_e (see Ref. 7). In the weak-field limit $B^* \ll 1$ ($B^* = B/B_{\text{cr}}$ and $B_{\text{cr}} = 4.414 \times 10^{13}$ G is the electron critical field), the equation of state (EOS) can be written in the polytropic form,

$$P_e = K\rho^\Gamma , \quad (3)$$

where K and Γ are constants, in the following two limiting cases: 1. For non-relativistic electrons, $\rho \ll 10^6$ g cm $^{-3}$,

$$\Gamma = \frac{5}{3}, \quad K = \frac{1.0036 \times 10^{13}}{(A/Z)^{5/3}} \text{ cgs} , \quad (4)$$

where A and Z are the number of nucleons and the number of protons, respectively.

2. For extremely relativistic electrons, $\rho \gg 10^6$ g cm $^{-3}$,

$$\Gamma = \frac{4}{3}, \quad K = \frac{1.2435 \times 10^{15}}{(A/Z)^{4/3}} \text{ cgs} . \quad (5)$$

Be note that, for a given nucleus with proton number Z and nucleon number A , the relation of $Y_e = Y_p = Z/A$ always approximately holds, where Y_p is the proton fraction; for an ideal neutron-proton-electron (npe) gas, $Y_e = Y_p = \frac{n_e}{n_B} = \frac{n_e}{n_p+n_n} \approx \frac{n_e}{n_n}$, where n_e , n_p , n_n and n_B are the electron number density, proton number density, neutron number density and baryon number density, respectively.

In this paper, we focus on the interior of a magnetar where electrons are degenerate and relativistic. The effects of a strong magnetic field on the equilibrium composition of a NS have been shown in detail in previous studies (e.g., Ref. 8, 9). In accordance with the popular point of view on the electron pressure in strong magnetic fields, the stronger the magnetic field, the lower the electron pressure becomes. With respect to this viewpoint, we cannot directly verify it by the experiment in actual existence, owing to the lack of such high-value magnetic fields on the earth. After a careful check, we found that popular methods of calculating the Fermi energy of electrons are contradictory to the quantization of electron Landau levels. In an extremely strong magnetic field, the Landau column becomes a very long and very narrow cylinder along the magnetic field. By introducing the Dirac δ -function, we obtain

$$\frac{4\pi}{3B^*} \left(\frac{m_e c}{h}\right)^3 (\gamma_e)^4 \int_0^1 \left(1 - \frac{1}{\gamma_e^2} - \chi^2\right)^{\frac{3}{2}} d\chi - 2\pi\gamma_e \left(\frac{m_e c}{h}\right)^3 \sqrt{2B^*} = N_A \rho Y_e, \quad (6)$$

where χ and γ_e are two non-dimensional variables, defined as $\chi = (\frac{p_z}{m_e c}) / (\frac{E_F(e)}{m_e c^2}) = p_z c / E_F(e)$ and $\gamma_e = E_F(e) / m_e c^2$, respectively; $1/\gamma_e^2$ is the modification factor; h and N_A are the Planck constant and Avogadro constant, respectively (see Ref. 10, 11). Solving Eq.(6) gives a concise formula for $E_F(e)$ in superhigh magnetic fields,

$$E_F(e) \simeq 43.44 \left(\frac{B}{B_{\text{cr}}}\right)^{1/4} \left(\frac{\rho}{\rho_0} \frac{Y_e}{0.0535}\right)^{\frac{1}{4}} \text{ MeV}, \quad (7)$$

where $\rho_0 = 2.8 \times 10^{14} \text{ g cm}^3$ is the standard nuclear density (see Ref. 11).

The remainder of this paper is organized as follows: in Section 2, on the basis of our previous work, we deduce an equation involving P_e , ρ , B and Y_e , which is suitable for strong magnetic fields; in Section 3, we take into account QED effects on EOSs of different matter systems, and discuss an anisotropy of the total pressure of ideal npe gas due to strong magnetic fields; in Section 4, we present a dispute on P_e in superhigh magnetic fields, and finally we summarize our findings with conclusions in Section 5.

2. Pressure of degenerate and relativistic electrons

The relativistic Dirac-Equation for the electrons in a uniform external magnetic field along the z -axis gives the electron energy level

$$E_e = [m_e^2 c^4 (1 + \nu \frac{2B}{B_{\text{cr}}}) + p_z^2 c^2]^{\frac{1}{2}}, \quad (8)$$

where the quantum number ν is given by $\nu = n + \frac{1}{2} + \sigma$ for the Landau level $n = 0, 1, 2, \dots$, spin $\sigma = \pm \frac{1}{2}$ (see Ref. 12), and the quantity p_z is the z -component

4 Authors' Names

of the electron momentum and may be treated as a continuous function. Combining $B_{cr} = m_e^2 c^3 / e \hbar$ with $\mu'_e = e \hbar / 2 m_e c$ gives

$$E_e^2 = m_e^2 c^4 + p_z^2 c^2 + 2 \nu 2 m_e c^2 \mu'_e B \quad , \quad (9)$$

where μ'_e is the magnetic moment of an electron.

For the convenience of the following calculations, we define the electron momentum perpendicular to the magnetic field, $p_\perp = m_e c (2 \nu B^*)^{\frac{1}{2}}$. Then, Eq.(9) can be rewritten as,

$$E_e^2 = m_e^2 c^4 + p_z^2 c^2 + p_\perp^2 c^2 \quad , \quad (10)$$

The maximum electron Landau level number n_{max} is uniquely determined by the condition $[p_F(z)c]^2 \geq 0$ (see Ref. 9), where $p_F(z)$ is the Fermi momentum along the z -axis. The expression for n_{max} is

$$\begin{aligned} n_{\max}(\sigma = -\frac{1}{2}) &= \text{Int}[\frac{1}{2B^*}[(\frac{E_F(e)}{m_e c^2})^2 - 1 - (\frac{p_z}{m_e c})^2]] \quad , \\ n_{\max}(\sigma = \frac{1}{2}) &= \text{Int}[\frac{1}{2B^*}[(\frac{E_F(e)}{m_e c^2})^2 - 1 - (\frac{p_z}{m_e c})^2] - 1] \quad , \end{aligned} \quad (11)$$

where $\text{Int}[x]$ denotes an integer value of the argument x . Correspondingly, the expression for ν_{max} can be expressed as

$$\begin{aligned} \nu_{\max}(\sigma = -\frac{1}{2}) &= \text{Int}[\frac{1}{2B^*}[(\frac{E_F(e)}{m_e c^2})^2 - 1 - (\frac{p_z}{m_e c})^2] + \frac{1}{2} - \frac{1}{2}] \quad , \\ &= \text{Int}[\frac{1}{2B^*}[(\frac{E_F(e)}{m_e c^2})^2 - 1 - (\frac{p_z}{m_e c})^2]] \quad , \\ \nu_{\max}(\sigma = \frac{1}{2}) &= \text{Int}[\frac{1}{2B^*}[(\frac{E_F(e)}{m_e c^2})^2 - 1 - (\frac{p_z}{m_e c})^2] - 1 + \frac{1}{2} + \frac{1}{2}] \quad , \\ &= \text{Int}[\frac{1}{2B^*}[(\frac{E_F(e)}{m_e c^2})^2 - 1 - (\frac{p_z}{m_e c})^2]] \quad . \end{aligned} \quad (12)$$

From Eq.(12), it's obvious that

$$\nu_{\max}(\sigma = -\frac{1}{2}) = \nu_{\max}(\sigma = \frac{1}{2}). \quad (13)$$

However, the electron Fermi momentum is the maximum of electron momentum. The physics on the condition $[p_F(z)c]^2 \geq 0$ in Ref. 9 includes that: n_{max} is determined by $E_F(e)$ and p_z when B is given; for a given Landau level number n , p_z always has the maximum $p_z(max)$ corresponding to n ; in the same way, when p_z is given, n also has the maximum n_{max} corresponding to p_z . Maybe n'_{max} corresponding to $p_z = 0$ is most meaningful to us, and so is $p_F(z)$ corresponding to $n = 0$ (when $n = 0$, the spin is antiparallel to B , and $\sigma = -\frac{1}{2}$).

According to the definition of $E_F(e)$ in Eq.(2), we obtain $E_F(e) \equiv p_F(e)c$ if electrons are super-relativistic ($E_F(e) \gg m_e c^2$). In the presence of a superhigh

magnetic field $B \gg B_{\text{cr}}$, $E_{\text{F}}(e) \gg m_e c^2$, hence we have the following approximate relation

$$\nu_{\text{max}}(\sigma = -\frac{1}{2})' = \nu_{\text{max}}(\sigma = \frac{1}{2})' \simeq \text{Int}[\frac{1}{2B^*}[(\frac{E_{\text{F}}(e)}{m_e c^2})^2]] . \quad (14)$$

From the analysis above, we can calculate the maximum of electron momentum perpendicular to the magnetic field by

$$p_{\perp}^2(\text{max})c^2 = 2\nu'_{\text{max}}2m_e c^2 \mu'_e B , \quad (15)$$

where the relation of $2\mu'_e B_{\text{cr}}/m_e c^2 = 1$ is used. Inserting Eq.(14) into Eq.(15) gives

$$\begin{aligned} p_{\perp}^2(\text{max})c^2 &= 2 \times \frac{1}{2B^*} (\frac{E_{\text{F}}(e)}{m_e c^2})^2 \times 2m_e c^2 \mu'_e B \\ &\simeq B_{\text{cr}} \times (\frac{E_{\text{F}}(e)}{m_e c^2})^2 \times 2m_e c^2 \frac{e\hbar}{2m_e c} \\ &= \frac{m_e^2 c^3}{e\hbar} \times (\frac{E_{\text{F}}(e)}{m_e c^2})^2 \times 2m_e c^2 \frac{e\hbar}{2m_e c} = E_{\text{F}}^2(e) . \end{aligned} \quad (16)$$

Thus, we gain

$$\begin{aligned} p_{\perp}(\text{max}) &= p_{\text{F}}(e) \simeq \frac{E_{\text{F}}(e)}{c} \\ &= 43.44 \times (\frac{Y_e}{0.0535} \frac{\rho}{\rho_0} \frac{B}{B_{\text{cr}}})^{\frac{1}{4}} \text{MeV}/c \quad (B^* \geq 1) . \end{aligned} \quad (17)$$

As pointed out above, when $n = 0$, the electron Landau level is non-degenerate, and p_z has its maximum $p_z(\text{max})$,

$$\begin{aligned} p_z(\text{max}) &= p_{\text{F}}(e) \simeq \frac{E_{\text{F}}(e)}{c} \\ &= 43.44 \times (\frac{Y_e}{0.0535} \frac{\rho}{\rho_0} \frac{B}{B_{\text{cr}}})^{\frac{1}{4}} \text{MeV}/c \quad (B^* \geq 1) . \end{aligned} \quad (18)$$

From Eq.(17) and Eq.(18), it's obvious that $p_z(\text{max}) = p_{\perp}(\text{max}) = p_{\text{F}}(e)$, which implies the electron pressure along the magnetic field, $P_z(e)$, is equal to the electron pressure in the direction perpendicular to the magnetic field, $P_{\perp}(e)$. The reason for this is that in the interior of a magnetar, electrons are degenerate and super-relativistic, and can be approximately treated as an ideal Fermi gas with equivalent pressures in all directions, though the existence of Landau levels. The equation of P_e in a superhigh magnetic field is consequently given by

$$\begin{aligned} P_e &= \frac{1}{3} \frac{2}{h^3} \int_0^{p_{\text{F}}(e)} \frac{p_e^2 c^2}{(p_e^2 c^2 + m_e^2 c^4)^{1/2}} 4\pi p_e^2 dp_e \\ &= \frac{m_e c^2}{\lambda_e^3} \phi(x_e) = 1.412 \times 10^{25} \phi(x_e) \text{ dynes cm}^{-2} , \end{aligned} \quad (19)$$

where $\lambda_e = \frac{h}{m_e c}$ is the electron Compton wavelength, and $\phi(x_e)$ is the polynomial of a non-dimensional variable x_e ($x_e = \frac{p_{\text{F}}(e)}{m_e c} \simeq \frac{E_{\text{F}}(e)}{m_e c^2} = 86.77 \times (\frac{\rho}{\rho_0} \frac{B}{B_{\text{cr}}} \frac{Y_e}{0.0535})^{\frac{1}{4}}$),

$$\phi(x_e) = \frac{1}{8\pi^2} [x_e(1+x_e^2)^{\frac{1}{2}} (\frac{2x_e^2}{3} - 1) + \ln[x_e + (1+x_e^2)^{\frac{1}{2}}]] . \quad (20)$$

6 Authors' Names

When $\rho \geq 10^7 \text{ g cm}^{-3}$, $x_e \gg 1$, and $\phi(x_e) \rightarrow \frac{x_e^4}{12\pi^2}$. Thus, Eq.(19) can be rewritten as

$$P_e \simeq 6.266 \times 10^{30} \left(\frac{\rho}{\rho_0} \frac{B}{B_{\text{cr}}} \frac{Y_e}{0.0535} \right) \text{ dyne cm}^{-2} \quad . \quad . \quad (21)$$

Comparing Eq.(21) with Eq.(7), it's easy to see that $P_e \propto E_{\text{F}}^4(e)$. Employing Eq.(21), we plot the schematic diagrams of P_e vs. B , as shown in Fig.1.

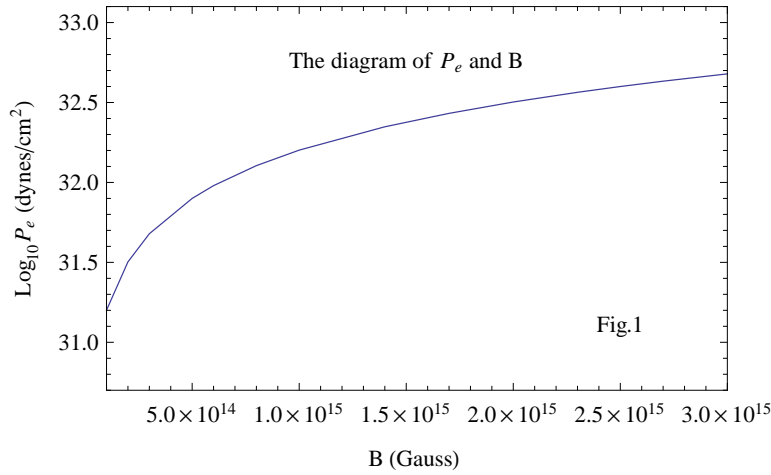


Fig. 1. The electron pressure dependence of the magnetic field strength when $\rho = \rho_0$ and $Y_e = 0.06$. When B is assumed to be $(1.0 \times 10^{14} \sim 3.0 \times 10^{15}) \text{ G}$, P_e is $(1.592 \times 10^{31} \sim 4.776 \times 10^{32} \text{ dynes cm}^{-2})$, correspondingly.

From Fig.1, P_e increases sharply with increasing B when the values of Y_e and ρ are given. We also present a schematic illustration of P_e as a function of ρ in different magnetic fields, as shown in Fig.2.

As pointed in our previous study (see Ref. 10), the high Fermi energy of electrons could be supplied by the release of the magnetic field energy. Since P_e is proportional to $E_{\text{F}}^4(e)$, and the later increases with increasing B , then the former also increases with increasing B naturally. Although we have presented a reasonable explanation for high-value P_e here, an important issue of electron distributions among different Landau levels in a superhigh magnetic field remains unsolved. According to a popular viewpoint that the stronger the magnetic field, the smaller the maximum electron Landau level number n_{max} becomes, the number of electrons congregating in an exciting level ($n \geq 1$) decrease with increasing B , if $B \gg B_{\text{cr}}$, then $n_{\text{max}} = 1$ or 2, and the overwhelming majority of electrons occupy in the ground level $n = 0$, which causes a decrease in the momentum p_z , as well as a decrease in the momentum p_{\perp} . However, the Dirac Delta-function $\delta(\frac{p_{\perp}}{m_e c} - [2(n + \sigma + \frac{1}{2})B^*]^{\frac{1}{2}})$ obviously tells us that, given a Landau level number n , both the momentum $p_{\perp}(n) \sim m_e c [2(n + \sigma + \frac{1}{2})B^*]^{\frac{1}{2}}$

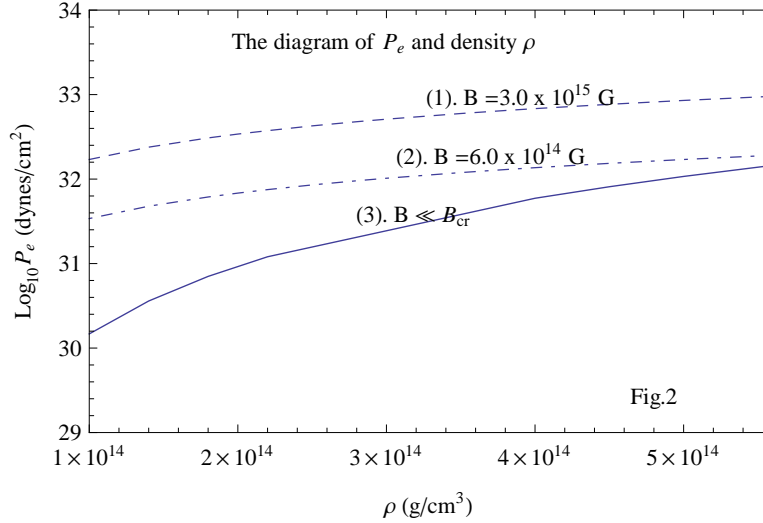


Fig. 2. The electron pressure dependence of the matter density in different magnetic fields when $Y_e = 0.06$. When ρ is assumed to be $(1.0 \times 10^{14} \sim 5.6 \times 10^{14}) \text{ g cm}^{-3}$, the ranges of P_e are $1.471 \times 10^{30} \sim 1.454 \times 10^{32} \text{ dynes cm}^{-2}$, $3.411 \times 10^{31} \sim 1.910 \times 10^{32} \text{ dynes cm}^{-2}$, and $1.521 \times 10^{32} \sim 8.545 \times 10^{32} \text{ dynes cm}^{-2}$, respectively, corresponding to $B^* \ll 1$, $B = 6.0 \times 10^{14} \text{ G}$ and $B = 3.0 \times 10^{15} \text{ G}$, respectively. The solid line is obtained from Eq.(3) for the relativistic electrons (see Section 1).

and the magnetic energy $E_B(n) \sim p_{\perp}(n)c \sim m_e c^2 [2(n + \sigma + \frac{1}{2})B^*]^{\frac{1}{2}}$ increase with increasing B , which implies more electrons contribute to $p_{\perp}(n)$ and $E_B(n)$. Thus, given a Landau level n , the number of electrons should increase with increasing B , rather than decrease with B . With respect to $\Delta p_{\perp}(n, n+1)$, the difference of p_{\perp} between two adjacent Landau levels, when the Landau level number n is given, $\Delta p_{\perp}(n, n+1)$ increases with increasing B ; when B is given, $\Delta p_{\perp}(n, n+1)$ decreases with increasing n , and if $n \rightarrow n_{max}$, then $\Delta p_{\perp}(n, n+1)$ is too small to be taken into account. The increase of $E_F(e)$, together with the increase of number of electrons populating in the vicinity of Fermi surface, can result in an increase in the electron capture (EC) rate in the interior of a magnetar. The extreme activity and instability of a magnetar may be explained by high-value $E_F(e)$, and the released thermal energy in the EC process could be the source of magnetars' soft X/ γ -ray radiations (see Ref. 11, 13, 15).

3. The QED effects on equation of state

A superhigh magnetic field is intriguing in the physical context because some interesting phenomena would be expected from the quantum electrodynamic (QED) effects. One of the QED phenomena is the vacuum polarization, which causes large energy splitting of Landau levels, modifies the dielectric properties of the medium,

induces resonant conversion of photon modes (e.g., see Ref. 14, 16, 17), and decreases the equivalent width of the ion cyclotron line making the line more difficult to observe (see Ref. 18).

The observations display the presence of the hard X-ray spectra tails in magnetars, recently detected by XMM, ASCA, RXTE and INTEGRAL (e.g., see Ref. 19, 20, 21, 26, 27, 28). Some authors have tried to interpret these observations by employing Resonant Compton Scattering (RCS) by relativistic electrons in superhigh magnetic fields (e.g., see Ref. 29, 30, 31, 32, 33, 34). RCS is also an interesting phenomenon due to QED effects, and has been treated as a leading emission mechanism for the hard X-ray radiation of magnetars. With respect to the QED effects on the spin-down and heat evolution of magnetars, for details, see a recent review of Ref. 25.

However, as an alternative, in this work, we shall concentrate on the QED effects on different matter systems of a magnetar, and discuss the star's deformation due to strong magnetic fields. This Section is composed of three sub-sections. For each subsection we present different methods and considerations.

3.1. *The QED effects on the EOS of BPS model*

Considering shell effects on the binding energy of a given nucleus, Salpeter (1961) first calculated the composition and EOS in the region of $10^7 - 3.4 \times 10^{11} \text{ g cm}^{-3}$ (see Ref. 35). By introducing the lattice energy, Baym, Pethick and Sutherland (hereafter BPS model) improved on Salpeter's treatment, and described the nuclear composition and EOS for catalyzed matter in complete thermodynamic equilibrium below neutron drop $\rho_d \sim 4.4 \times 10^{11} \text{ g cm}^{-3}$ energy (see Ref. 36, 7).

Here, we shall not discuss electrons in the low density regime $10^4 \sim 10^6 \text{ g cm}^{-3}$, because the electrons are nonrelativistic, and EOS may be treated via a magnetic Thomas-Fermi (TF) type of model for a lattice of electrons and ${}^{56}_{26}\text{Fe}$ nuclei (see Ref. 37). Since we are concerned about the role of magnetic fields on EOS, a qualitative analysis of magnetic influence depending on the details of the nuclear model will not be presented here. Also, we'll utilize the simple BPS model, and no longer consider other more complicated models (e.g., the model in Ref. 38, in which the EOS is quite distinct from that of BPS model). We'll assume an isotropic and homogenous matter pressure P of this system. An anisotropy of the total pressure P_{tot} of the system due to a strong magnetic field will not be discussed in this subsection.

According to BPS model, the matter energy density is given by

$$\varepsilon = n_N(W_N(A, Z) + \varepsilon_L(Z, n_e) + \varepsilon_e(n_e)) \quad , \quad (22)$$

where n_N is the number density of nuclei, $W_N(A, Z)$ is the mass-energy per nucleus (including the rest mass of Z electrons and A nucleons); ε_e is the free electron energy including the rest mass of electrons in a unit volume; ε_L is the *bcc* Coulomb lattice

energy per nucleus,

$$\varepsilon_L = -1.444Z^{2/3}e^2e^2n_e^{4/3} \quad , \quad (23)$$

where the relations of $n_N = n_B/A$ and $n_e = Zn_N$ are used. The matter pressure p of the system is given by

$$P = P_e + P_L = P_e + \frac{1}{3}\varepsilon_L \quad . \quad (24)$$

In the case of the weak-field limit $B^* \ll 1$, P_e in Eq.(24) is given by Eq.(5). For a magnetic field $B^* \gg 1$, P_e in Eq.(24) is given by Eq.(21). For the specific equilibrium nuclei (A, Z) in BPS model, we calculate the values of quantities $\rho_m, n_B(m), E_F(e)$ and P_e , as tabulated in Table 1.

Table 1. Values of $\rho_m, n_B(m), E_F(e)$ and P_e in BPS model below neutron drip.

Nuclei [†]	Y_e	ρ_m^0 g cm ⁻³	ρ_m^1 g cm ⁻³	$n_B^0(m)$ cm ⁻³	$n_B^1(m)$ cm ⁻³	$E_F^0(e)$ MeV	$E_F^1(e)$ MeV	P_e^0 dynes cm ⁻²	P_e^1 dynes cm ⁻²
⁵⁶ ₂₆ Fe	0.464	7.99×10 ⁶	4.67×10 ⁸	4.812×10 ³⁰	2.812×10 ³²	0.95	8.77	7.141×10 ²³	9.069×10 ²⁷
⁶² ₂₈ Ni	0.452	2.71×10 ⁸	1.68×10 ⁹	1.632×10 ³²	1.012×10 ³³	2.61	12.01	7.556×10 ²⁵	3.174×10 ²⁸
⁶⁴ ₂₈ Ni	0.437	1.31×10 ⁹	2.78×10 ⁹	7.949×10 ³²	1.674×10 ³³	4.31	13.59	5.980×10 ²⁶	5.087×10 ²⁸
⁶⁶ ₂₈ Ni	0.424	1.54×10 ⁹	No [‡]	9.274×10 ³²	No [‡]	4.45	No [‡]	7.049×10 ²⁶	No [‡]
⁸⁶ ₃₆ Kr	0.419	3.11×10 ⁹	3.87×10 ⁹	1.873×10 ³³	2.331×10 ³³	5.66	14.49	1.767×10 ²⁷	6.776×10 ²⁸
⁸⁴ ₃₄ Se	0.405	9.98×10 ⁹	1.14×10 ¹⁰	6.009×10 ³³	6.865×10 ³³	8.49	18.84	7.999×10 ²⁷	1.930×10 ²⁹
⁸² ₃₂ Ge	0.390	2.08×10 ¹⁰	2.10×10 ¹⁰	1.252×10 ³⁴	1.265×10 ³⁴	11.44	21.75	2.028×10 ²⁸	3.428×10 ²⁹
⁸⁰ ₃₀ Zn	0.375	5.91×10 ¹⁰	5.69×10 ¹⁰	3.559×10 ³⁴	3.426×10 ³⁴	14.08	27.62	7.741×10 ²⁸	8.925×10 ²⁹
⁷⁸ ₂₈ Ni	0.359	8.21×10 ¹⁰	8.13×10 ¹⁰	4.944×10 ³⁴	4.896×10 ³⁴	20.01	28.86	1.132×10 ²⁹	1.221×10 ³⁰
¹²⁶ ₄₄ Ru	0.349	1.19×10 ¹¹	1.20×10 ¹¹	7.166×10 ³⁴	7.226×10 ³⁴	20.20	31.59	1.789×10 ²⁹	1.753×10 ³⁰
¹²⁴ ₄₂ Mo	0.339	1.66×10 ¹¹	1.67×10 ¹¹	9.996×10 ³⁴	1.006×10 ³⁵	20.50	34.05	2.678×10 ²⁹	2.366×10 ³⁰
¹²² ₄₀ Zr	0.328	2.49×10 ¹¹	2.50×10 ¹¹	1.499×10 ³⁵	1.506×10 ³⁵	22.89	37.32	4.404×10 ²⁹	2.428×10 ³⁰
¹²⁰ ₃₈ Sr	0.317	3.67×10 ¹¹	3.08×10 ¹¹	2.210×10 ³⁵	2.216×10 ³⁵	25.20	40.77	7.052×10 ²⁹	4.871×10 ³⁰
¹²² ₃₈ Sr	0.311	3.89×10 ¹¹	3.90×10 ¹¹	2.342×10 ³⁵	2.348×10 ³⁵	25.90	41.20	7.455×10 ²⁹	5.120×10 ³⁰
¹¹⁸ ₃₆ Kr	0.305	4.41×10 ¹¹	4.41×10 ¹¹	2.656×10 ³⁵	2.656×10 ³⁵	26.20	42.28	7.805×10 ²⁹	5.692×10 ³⁰

In this Table the signs of ‘0’ and ‘1’ denote $B^* \ll 1$ and $B^* = 100$, respectively, and $n_B(m)$ is the maximum equilibrium baryon number density, corresponding to the maximum equilibrium density ρ_m at which the nuclide is present. The sign ‘†’ denotes that the first masses are known experimentally (see Ref. 39), and the remainder are from the Jänecke-Gravey-Kelson mass formula (see Ref. 40). The sign ‘‡’ denotes that ⁶²₂₈Ni is found to be absent from the equilibrium nucleus sequence, so is not presented. Furthermore, all digits in Column 3 and Column 4 of this Table are cited from Lai and Shapiro (1991) (see Ref. 9). From Table 1, it’s obvious that the electron pressure P_e , as well as $E_F(e)$, increases with matter density and magnetic field, and a strong magnetic field alters the nucleus transition densities for the low- A nuclei. In a strong magnetic field, as the density increases, the nuclei become increasingly saturated with neutrons, however, neutron drip occurs at the same density because we adopts a nearly constant minimum Gibbs free energy per nucleon, $g_{min} = m_n c^2$. From Table 1, the calculated values of P_e are in the

10 Authors' Names

range of $9.069 \times 10^{27} \sim 5.692 \times 10^{30}$ dynes cm^{-2} corresponding to a density range of $4.67 \times 10^8 \sim 4.41 \times 10^{11}$ when $B^* = 100$. Based on this Table we plot four schematic sub-diagrams of QED effects on the EOS, as shown in Fig.3.

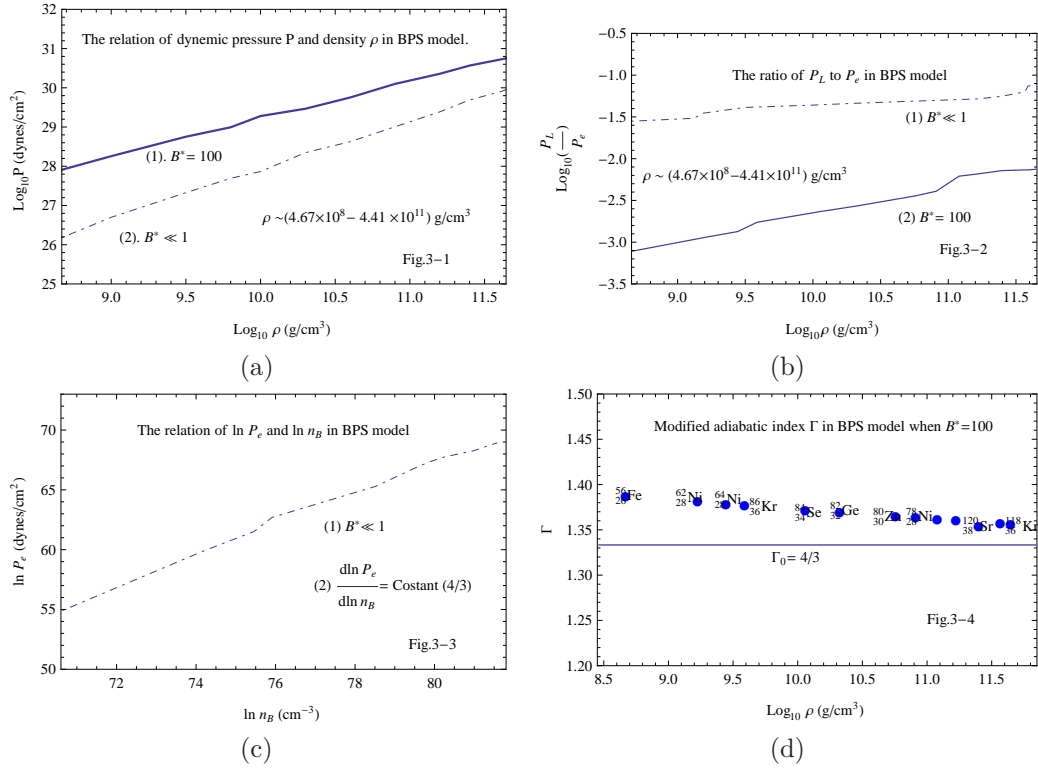


Fig. 3. The QED effects on the EOS of BPS model below neutron drip. Sub-diagrams Fig.3-1, Fig.3-2, Fig.3-3 and Fig.3-4 give P versus ρ , P_L/P_e versus ρ , $\ln P_e$ versus $\ln n_B$ and Γ versus ρ for specific nucleus, respectively. Here, ρ denotes the maximum equilibrium density, Γ is the modified adiabatic index (e.g., unlike the adiabatic index Γ_0 in the weak-field limit, Γ is an adiabatic index after taking into account magnetic effects).

From the sub-diagram Fig.3-1, the matter pressure P described by Eq.(24) increases obviously with density ρ for both in a superhigh magnetic field and in the weak-field limit. Furthermore, given a density ρ , the value of P in the case of the former ($B^* = 100$) is bigger than that of P in the case of the latter ($B^* \ll 1$), which can be easily seen from the curves of Fig.3-1. From the sub-diagram Fig.3-2, the ratios of P_L to P_e are about 10^{-2} and 10^{-3} , respectively, corresponding to $B^* = 100$ and $B^* \ll 1$, respectively. Therefore, one can infer that the contribution of P_L to the matter pressure P can be ignored if $B^* \geq 100$. In the sub-diagram Fig.3-3, we fit a curve of $\ln P_e$ versus $\ln n_B$ in the weak-field limit. Since the electrons are relativistic, the adiabatic index Γ (i.e., the slope of the curve) is a constant of $4/3$, which is the

standard relativistic value. In a strong magnetic field $B^* = 100$, due to the changes of P_e and ρ_m , the values of modified Γ are slightly higher than the constant of $4/3$, i.e, $\Gamma \equiv \ln P_e / \ln n_B \simeq 1.36 \sim 1.39$, as illustrated in the sub-diagram Fig.3-4.

3.2. The QED effects on the EOS of BBP model

In the domain above neutron drip, as the matter density increases and the nuclei become more neutron rich, and the system becomes a mixture of nuclei, free neutrons, and electrons. When a critical value of baryon number density is reached, the nuclei disappear, essentially by merging together. Here we shall focus on the EOS of Baym, Bethe, and Pethick (1971) (see Ref. 41)(hereinafter BBP), which describes such a system more successfully, compared with other models.

In this subsection, we'll also assume an isotropic and homogenous matter pressure P of this system, and will not discuss an anisotropy of the total pressure P_{tot} of the system due to a strong magnetic field.

In the work by BBP, the major improvement was the introduction of a compressible liquid drop model of the nuclei (see Ref. 41). The energy density of BBP model is written as

$$\varepsilon = \varepsilon_e(n_e) + n_N(W_N + W_L) + n_n(1 - V_N n_N)W_n \quad , \quad (25)$$

where n_n is the number density of neutrons outside of nuclei (hereinafter neutron gas), and the new feature is the dependence on the volume of a nucleus V_N , which decreases with the outside pressure of the neutron gas. The baryon number density in this model is

$$n_B = An_N + (1 - V_N n_N)n_n \quad , \quad (26)$$

where $V_N n_N$ and $1 - V_N n_N$ are the fraction of volume occupied by nuclei, and the fraction occupied by the neutron gas, respectively. The matter pressure p in BBP model is given by

$$P = P_n + P_e + P_L \quad . \quad (27)$$

In the original work of BBP (1971), the three terms of P_n , P_e , P_L in Eq.(27) are calculated by $P_n = n_n^2 \frac{\partial E_n}{\partial n_n}$, $P_e = n_e^2 \frac{\partial E_e}{\partial n_e}$, and $P_L = n_N^2 \frac{\partial E_L}{\partial n_N}$, respectively. Ignoring the details of calculations, we list the values of chemical potentials μ_e and μ_n in Table 2, and cite the results of P_n , P_e and P in plotting Fig.4 from BBP (1971) and the review of Canuto (1974)(see Ref. 42).

In a superhigh magnetic field, according to our model, the three pressure terms in Eq.(27) are approximately treated as follows: Since the ratio of P_L/P is $\sim 10^{-3} - 10^{-4}$, the contribution of negative lattice pressure P_L to the total dynamic pressure P can be neglected; As in the magnetic BPS model, the electron pressure P_e is also given by Eq.(21); In order to calculate the neutron pressure P_n , at first, ignoring the neutrino chemical potential μ_ν , we determine μ_n via β -equilibrium under a uniform superhigh magnetic field,

$$\mu_e + \mu_p + m_p c^2 = \mu_n + m_n c^2 \quad , \quad (28)$$

where μ_e is the electron chemical potential, i.e., the electron Fermi energy $E_F(e)$, including the rest-mass energy $m_e c^2$, μ_p is the proton chemical potential, i.e., the proton Fermi energy, not including the rest-mass energy $m_p c^2$ (notice that in BBP model the protons do not contribute the matter pressure because μ_p is negative), and μ_n is also called the neutron Fermi energy $E'_F(n)$, not including its rest-mass energy $m_n c^2$, $\mu_n = E'_F(n) = \frac{p_F^2(n)}{2m_n}$, secondly, by defining a non-dimensional variable $x_n = \frac{p_F(n)}{m_n c} = \frac{\sqrt{2m_n \mu_n}}{m_n c} = \sqrt{\frac{2\mu_n}{m_n c^2}}$, we gain the polynomial $\phi(x_n)$ of the variable x_n ,

$$\phi(x_n) = \frac{1}{8\pi^2} [x_n(1+x_n^2)^{\frac{1}{2}} (\frac{2x_n^2}{3} - 1) + \ln[x_n + (1+x_n^2)^{\frac{1}{2}}]] \quad , \quad (29)$$

where the neutrons are nonrelativistic (the density $\rho \ll 6 \times 10^{15}$ g cm $^{-3}$ in BBP model), then $x_e \ll 1$, and $\phi(x_n) \rightarrow \frac{1}{15\pi^2} (x_n^5 - \frac{5}{14}x_n^7 + \frac{5}{24}x_n^9)$; finally, following Shapiro & Teukolsky (1983)(hereafter ST, see Ref. 7), we can calculate the value of P_n by

$$P_n = \frac{m_n c^2}{\lambda_n^3} \phi(x_n) = 1.624 \times 10^{38} \frac{1}{15\pi^2} (x_n^5 - \frac{5}{14}x_n^7 + \frac{5}{24}x_n^9) \text{ dynes cm}^{-2} \quad , \quad (30)$$

where $\lambda_n = \frac{h}{m_n c}$ is the Compton wavelength of a neutron. In Table 2 we present the values of μ_e and μ_n corresponding to different magnetic fields in BBP model.

 Table 2. Values of μ_e and μ_n in magnetic BBP model.

ρ (g cm $^{-3}$)	A	Z	$n_N \times 10^{-6}$ (fm $^{-3}$)	n_B (cm $^{-3}$)	Y_e^\dagger	μ_e^0 (MeV)	μ_e^1 (MeV)	μ_e^2 (MeV)	μ_n^0 (MeV)	μ_n^1 (MeV)	μ_n^2 (MeV)
4.66×10^{11}	127	40	2.02	2.806×10^{35}	0.2879	26.31	35.54	42.26	0.14	9.37	16.09
6.61×10^{11}	130	40	2.13	3.981×10^{35}	0.2315	26.98	36.72	43.67	0.37	10.11	17.06
8.79×10^{11}	134	41	2.23	5.293×10^{35}	0.1727	27.51	36.86	43.83	0.55	9.90	16.87
1.20×10^{12}	137	42	2.34	7.226×10^{35}	0.1360	28.13	37.32	44.38	0.75	9.94	17.10
1.47×10^{12}	140	42	2.43	8.852×10^{35}	0.1153	28.58	37.67	44.80	0.91	10.10	17.13
2.00×10^{12}	144	43	2.58	1.204×10^{36}	0.0921	29.33	38.47	45.74	1.15	10.29	17.56
2.67×10^{12}	149	44	2.74	1.608×10^{36}	0.0749	30.15	39.26	46.69	1.42	10.53	17.96
3.51×10^{12}	154	45	2.93	2.114×10^{36}	0.0624	31.05	40.17	47.76	1.71	10.83	18.42
4.54×10^{12}	161	46	3.14	2.734×10^{36}	0.0528	32.02	41.08	48.86	2.01	11.07	18.85
6.25×10^{12}	170	48	3.45	3.764×10^{36}	0.0439	33.43	42.52	50.56	2.45	11.54	19.58
8.38×10^{12}	181	49	3.82	5.046×10^{36}	0.0371	34.98	43.84	52.14	2.91	11.71	20.07
1.10×10^{13}	193	51	4.23	6.624×10^{36}	0.0326	36.68	45.44	54.03	3.41	12.17	20.76
1.50×10^{13}	211	54	4.84	9.033×10^{36}	0.0289	39.00	47.64	56.65	4.07	12.71	21.72
1.99×10^{13}	232	57	5.54	1.198×10^{37}	0.0264	41.56	49.99	59.45	4.77	13.20	22.66
2.58×10^{13}	257	60	6.36	1.554×10^{37}	0.0246	44.37	52.41	62.32	5.51	13.55	23.46
3.44×10^{13}	296	65	7.52	2.071×10^{37}	0.0236	48.10	55.73	66.28	6.47	14.10	24.65
4.68×10^{13}	354	72	9.12	2.818×10^{37}	0.0233	52.95	59.99	71.38	7.67	14.71	26.10
5.96×10^{13}	421	78	10.7	3.589×10^{37}	0.0235	57.56	64.38	76.56	8.77	15.90	27.77
8.01×10^{13}	548	89	13.1	4.824×10^{37}	0.0242	64.32	69.25	82.35	10.36	15.29	28.39
9.83×10^{13}	683	100	15.0	5.920×10^{37}	0.0253	69.81	73.76	87.72	11.66	15.61	29.57
1.30×10^{14}	990	120	17.8	7.828×10^{37}	0.0233	78.58	80.57	95.82	13.77	15.76	30.01
$1.72^{\ddagger} \times 10^{14}$	1640	157	19.6	1.035×10^{38}	0.0297	88.84	88.28	104.98	16.39	15.83	32.53
2.00×10^{14}	2500	210	18.8	1.205×10^{38}							
2.26×10^{14}	4330	290	15.4	1.361×10^{38}							
2.39×10^{14}	7840	445	11.0	1.439×10^{38}							

In this Table, the signs of '0', '1' and '2' denote $B^* \ll 1$, $B^* = 50$ and $B^* = 100$, respectively, and the data of columns 1, 2, 3, 4, 7 and 10 are from Table 2 of Canuto (1974)(see Ref. 42). The sign '†' denotes the electron fraction Y_e is given by $Y_e = Y_p = \frac{Zn_N}{n_B} \simeq \frac{Zn_N}{\rho/m_u}$, where $m_u = 1.66057 \times 10^{-24}$ g is the atom-mass unit because n_B always can be treated as an invariable quantity in spit of a strong magnetic field. The sign '‡' denotes that the EOS of BBP model has been criticized by some authors (e.g., see Ref. 42, 7), due to a monotonic and arbitrary increase of Z with A , which causes the relation of P and ρ to be changed not much, so we stop listing the related calculations in the higher density region, $\rho \geq 1.72 \times 10^{14}$ g cm⁻³.

The values of μ_n are obtained from Eq.(28) ignoring the changes of kinetic energies and potential energies of protons in nuclei and the transformations between protons and neutrons caused by strong magnetic fields (i.e., keeping μ_p and Y_p or Y_e constant). In a superhigh magnetic field, the system under consideration is still a mixture of free neutrons, electrons, and nuclei. Since there is a lack of experimental data on the changes and transformations above, we still take the quantities μ_p and Y_p as constants approximately when calculating μ_e and μ_n . If $B \gg 10^{20}$ G, these ignorers are not permitted due to larger calculating errors. Note that such strong magnetic fields will no longer be taken into account according to our magnetar model (for details, see the following subsection). However, these ignorers can not affect our main result here that the values of μ_e and μ_n increase with increasing magnetic fields and densities. Based on Table 2 we plot four schematic sub-diagrams of QED effects on the EOS of BBP model, as shown in Fig.4.

From sub-diagrams Fig.4-1 and Fig.4-2, both P_e and P obviously increase with density ρ for the three cases. As in BPS model above, given a same density ρ , the stronger the magnetic field is, the higher the values of P_e and P become. However, the increments of P_e and P in the lower density region are larger than those in the higher density region. The main reason for this is that the increments of quantities μ_e and μ_n in the lower density region are larger than those in the higher density region, which can be easily seen in Table 2. In Fig.4-3 the curve of adiabatic index Γ and ρ in the weak-field limit is obtained by fitting with the data of Table 6 in Canuto (1974) (see Ref. 42). The key feature of the curve in this sub-diagram is that Γ decreases with increasing ρ firstly, and then increases with increasing ρ . This phenomenon can be explained as follows: Firstly, as the neutron drip density ρ_d is approached, the electrons are extremely relativistic, and the matter pressure is almost entirely due to electrons, therefore $\Gamma_0 = 4/3$; Secondly, slightly above ρ_d , the low-density neutron gas contributes appreciably to the density but not much to the matter pressure, and thus Γ falls sharply. This drop in BBP model is described as $\Gamma = \frac{4}{3}[1 - a(\rho - \rho_d)^{1/2}]$, where a is a positive constant. Thirdly, as the density increases (about $\rho \geq 10^{12}$ g cm⁻³), the free neutrons nevertheless contribute to an increasingly larger fraction of the matter pressure. According to our calculations, in a strong magnetic field, e.g., $B^* \geq 50$, when $\rho \sim 10^{12}$ g cm⁻³, $P_n/P \sim 0.1-0.2$, while $\rho \sim 10^{13} - 10^{14}$ g cm⁻³, then $P_n/P \sim 0.8 - 0.99$, assuming that ρ_d is unchanged.

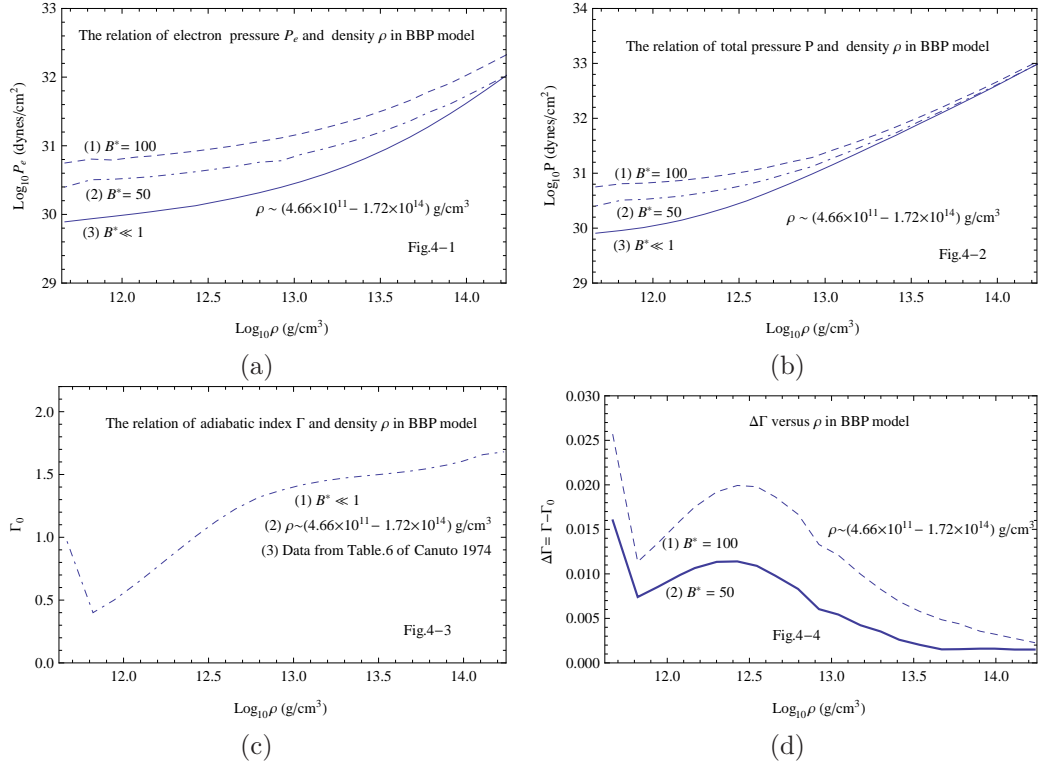


Fig. 4. The QED effects on the EOS of BBP model. Sub-diagrams Fig.4-1, Fig.4-2, Fig.4-3 and Fig.4-4 give P_e versus ρ , P versus ρ , Γ versus ρ , and $\Delta\Gamma$ versus ρ , respectively, for this EOS in different magnetic fields. The matter pressure P of this system is described by Eq.(27), assuming that μ_p and Y_e are invariant approximately.

In addition, Γ grows with increasing B and ρ slightly ($\Delta\Gamma \sim 10^{-2} - 10^{-3}$) due to an increase in P , as shown in Fig.4-4.

3.3. The QED effects on the EOS of ideal npe gas

In this subsection, we consider a homogenous ideal npe gas under β - equilibrium, and adopt ST approximation corresponding to the weak-field limit (see Ref. 7) as the main method to treat EOS of this system in the density range of $0.5\rho_0 \sim 2\rho_0$ where electrons are relativistic, neutrons and protons are non-relativistic. According to ST, when $\rho \gg 10^{13} \text{ g cm}^{-3}$, neutrons dominate in the interior of a NS, $\rho \approx m_n n_n$, then $n_n = 1.7 \times 10^{38} (\frac{\rho}{\rho_0}) \text{ cm}^{-3}$ (see Ref. 7); employing β - equilibrium and charge neutrality gives $n_p = n_e = 9.6 \times 10^{35} (\frac{\rho}{\rho_0})^2 \text{ cm}^{-3}$; β -equilibrium implies energy conservation and momentum conservation ($p_F(p) = p_F(e)$), we get $E_F(e) = \mu_n = E'_F(n) = p_F^2(n)/2m_n = 60 (\frac{\rho}{\rho_0})^{2/3} \text{ MeV}$, and $\mu_p = E'_F(p) = p_F^2(p)/2m_p =$

$1.9(\frac{\rho}{\rho_0})^{4/3}$ MeV; the isotropic matter pressure P is given by

$$\begin{aligned} P &= P_e + P_p + P_n \\ &= \frac{m_e c^2}{\lambda_e^3} \phi(x_e) + \frac{m_p c^2}{\lambda_p^3} \phi(x_p) + \frac{m_n c^2}{\lambda_n^3} \phi(x_n) \quad , \end{aligned} \quad (31)$$

where $x_p = \frac{p_F(p)}{m_p c} = \frac{\sqrt{2m_p \mu_p}}{m_p c} = \sqrt{\frac{2\mu_p}{m_p c^2}}$, the expression of $\phi(x_p)$ is completely similar to that of $\phi(x_n)$ (see Eq.(29)).

Based on the above results, we gain the following useful formulae:

$$\begin{aligned} P_p &= 1.169 \times 10^{30} \left(\frac{\rho}{\rho_0}\right)^{\frac{10}{3}} \text{ dynes cm}^{-2} \quad , \\ P_e &= 1.825 \times 10^{31} \left(\frac{\rho}{\rho_0}\right)^{\frac{8}{3}} \text{ dynes cm}^{-2} \quad , \\ P_n &= 6.807 \times 10^{33} \left(\frac{\rho}{\rho_0}\right)^{\frac{5}{3}} \text{ dynes cm}^{-2} \quad , \\ Y_e &= \frac{n_e}{n_p + n_n} \simeq \frac{n_e}{n_n} = 0.005647 \left(\frac{\rho}{\rho_0}\right) \quad . \end{aligned} \quad (32)$$

Be note that these formulae in Eq.(32) always hold approximately in an ideal npe gas when $B^* \ll 1$ and $\rho \sim 0.5\rho_0 - 2\rho_0$.

Our methods to treat EOS of an ideal npe gas (system) under β -equilibrium in superhigh magnetic fields are introduced as follows: Combining Eq.(7) with momentum conservation $p_F(p) = p_F(e)$ gives the chemical potential $\mu_p = E'_F(p) = 1.005 \left(\frac{B}{B_{cr}} \frac{\rho}{\rho_0} \frac{Y_e}{0.0535}\right)^{\frac{1}{2}}$ MeV, and the non-dimensional variable $x_p = \sqrt{\frac{2\mu_p}{m_p c^2}} \simeq 4.626 \times 10^{-2} \left(\frac{B}{B_{cr}} \frac{\rho}{\rho_0} \frac{Y_e}{0.0535}\right)^{\frac{1}{4}}$; From Eq.(28), we get the non-dimensional variable,

$$\begin{aligned} x_n &= \sqrt{\frac{1}{m_n c^2}} \left(2 \times (43.44 \left(\frac{B}{B_{cr}} \frac{\rho}{\rho_0} \frac{Y_e}{0.0535}\right)^{1/4} \right. \\ &\quad \left. - 1.29 + 1.005 \left(\frac{B}{B_{cr}} \frac{\rho}{\rho_0} \frac{Y_e}{0.0535}\right)^{1/2}\right)^{1/2} \quad . \end{aligned} \quad (33)$$

Thus, re-solving Eq.(31) gives the expression for the isotropic matter pressure P ,

$$\begin{aligned} P &= \frac{m_e c^2}{\lambda_e^3} \phi(x_e) + \frac{m_p c^2}{\lambda_p^3} \phi(x_p) + \frac{m_n c^2}{\lambda_n^3} \phi(x_n) \\ &= 6.266 \times 10^{30} \left(\frac{\rho}{\rho_0} \frac{B}{B_{cr}} \frac{Y_e}{0.0535}\right) + 2.324 \times 10^{26} \left(\frac{\rho}{\rho_0} \frac{B}{B_{cr}} \frac{Y_e}{0.0535}\right)^{\frac{5}{4}} \\ &\quad + 1.624 \times 10^{38} \frac{1}{15\pi^2} (x_n^5 - \frac{5}{14} x_n^7 + \frac{5}{24} x_n^9) \text{ dyne cm}^{-2} \quad , \end{aligned} \quad (34)$$

where x_n is determined by Eq.(33). The above equation always approximately hold in an ideal npe gas when $B^* \gg 1$ and $\rho \sim 0.5\rho_0 - 2\rho_0$.

In order to calculate the matter pressure P of an ideal npe gas in a super-high magnetic field, it's better to an analytical expression for Y_p (or Y_e) and B . Unfortunately, so far such an expression for Y_e and B has not been obtained yet.

Furthermore, some related researches are unauthentic, due to the lack of observational supports. For example, Chakrabarty et al.(1997) studied the gross properties of cold symmetric matter, and matter in β -equilibrium under the influences of superhigh magnetic fields using a relativistic Hartree theory (see Ref. 43). Their main conclusions are as follows: Superhigh magnetic fields $\sim 10^{20}$ G could exist in the interior of a NS; Y_e (or Y_p) is a strong function of B and ρ ; when an intense magnetic field is approached to the proton critical magnetic field, $B_{\text{cr}}^p \sim 1.48 \times 10^{20}$ G, the value of Y_p (or Y_e) is expected to be enhanced considerably; by strongly modifying the phase spaces of protons (electrons), the field of $B \sim 10^{20}$ G can bring on a substantial $n \rightarrow p$ conversion, and the system is hence transformed into highly proton-rich matter with distinctively softer EOS (see Ref. 43). However, up to date, there have been no observations indicating the existence of fields $B \geq 10^{17}$ G inside a NS as mentioned in Section 1 of this paper. To sum up, magnetic fields of such magnitude ($\sim 10^{20}$ G) inside NSs are unauthentic, and are not consistent with our magnetar model (see Ref. 5, Ref. 10, Ref. 13). In this letter, we assume the maximum magnetic field of a magnetar, $B \sim (3 - 4) \times 10^{15}$ G, in which n_B always keeps invariable, and the changes of n_p (or n_e) and n_n caused by the equilibrium process of $e^- + p \leftrightarrow n + \nu$ are too small to be considered. Thus, the magnetic effects on the proton (or electron) fraction also can be ignored. In Table 3 we present the values of $E_F(e)$, μ_p , μ_n and P in ideal npe gas corresponding to two cases: $B^* \ll 1$ and $B^* = 100$. The signs of '0' and '1' denote $B^* \ll 1$ and $B^* = 100$,

 Table 3. Values of $E_F(e)$, μ_p , μ_n and P in ideal $n - p - e$ gas corresponding to $B^* \ll 1$ and $B^* = 100$.

ρ (g cm $^{-3}$)	$E_F^0(e)$ (MeV)	μ_p^0 (MeV)	μ_n^0 (MeV)	$E_F^1(e)$ (MeV)	μ_p^1 (MeV)	μ_n^1 (MeV)	P^0 (dynes cm $^{-2}$)	P^1 (dynes cm $^{-2}$)
1.4×10^{14}	37.8	0.8	37.8	55.4	1.6	55.7	2.147×10^{33}	5.247×10^{33}
1.8×10^{14}	44.7	1.1	44.7	62.8	2.1	63.6	3.265×10^{33}	7.189×10^{33}
2.0×10^{14}	47.9	1.2	47.9	66.2	2.3	67.2	3.893×10^{33}	8.204×10^{33}
2.4×10^{14}	54.1	1.5	54.1	72.5	2.8	74.0	5.278×10^{33}	1.031×10^{34}
2.8×10^{14}	60.0	1.9	60.0	78.3	3.3	80.3	6.819×10^{33}	1.251×10^{34}
3.0×10^{14}	62.8	2.1	62.8	81.0	3.5	83.2	7.659×10^{33}	1.361×10^{34}
3.4×10^{14}	68.3	2.5	68.3	86.3	4.0	88.9	9.441×10^{33}	1.595×10^{34}
3.8×10^{14}	73.5	2.9	73.5	91.2	4.4	94.4	1.136×10^{34}	1.835×10^{34}
4.2×10^{14}	78.6	3.3	78.6	95.8	4.9	99.5	1.344×10^{34}	2.081×10^{34}
4.6×10^{14}	83.5	3.7	83.5	100.4	5.4	104.4	1.564×10^{34}	2.333×10^{34}
5.0×10^{14}	88.3	4.1	88.3	104.6	5.8	109.2	1.798×10^{34}	2.591×10^{34}
5.4×10^{14}	93.0	4.6	93.0	108.7	6.3	113.7	2.045×10^{34}	2.854×10^{34}
5.6×10^{14}	95.2	4.8	95.2	110.7	6.5	116.0	2.174×10^{34}	2.987×10^{34}

respectively. The values of P^0 and P^1 are obtained from Eq.(32) and Eq.(34), respectively. For simplicity, we ignore the change of Y_p (or Y_e) caused by magnetic effects when calculating P^1 . However, this **assumption** can not affect our main conclusion here that the dynamic pressure P increases with increasing B and ρ . Seeing from Table 3, for an ideal npe system, the chemical potentials of fermions, as well as matter pressure, increases with increasing B and ρ . Furthermore, the

ratios of P^1/P^0 are in the range of $\sim 2.4 - 1.4$ corresponding to a density range of $(1.4 \times 10^{14} - 5.6 \times 10^{14}) \text{g cm}^{-3}$, but the magnitudes of P^1 and P^0 are identical. Based on Table 3 we plot two schematic sub-diagrams of QED effects on EOS of this npe gas, as shown in Fig.5.

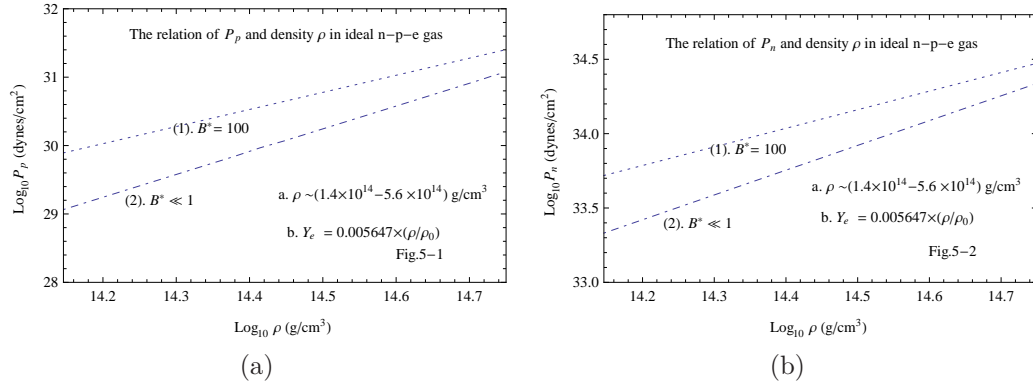


Fig. 5. The QED effects on P_p and P_n in ideal npe gas. Sub-diagrams Fig.5-1 and Fig. 5-2 give P_p versus ρ and P_n versus ρ , respectively, for an ideal npe gas in a superhigh magnetic field. Here the ST approximation is adopted in treating EOS of this system under β -equilibrium in the weak-field limit.

From sub-diagrams Fig.5-1 and Fig.5-2, both P_p and P_n increase obviously with density ρ and magnetic field B . As in magnetic BPS and BBP models above, given a same density ρ , the values of P_p and P_n in a superhigh magnetic field (e.g., $B^* = 100$) are higher than those in the weak-field limit.

As we know, in an ideal npe system under strong magnetic fields, there is a positive correlation between the total matter energy density, ϵ , and the total matter pressure, P ,

$$P = -\frac{\partial \epsilon / n}{\partial \frac{1}{n}} = n^2 \frac{\partial \epsilon / n}{\partial n}, \quad (35)$$

where n is equivalent to the number density of baryons, P includes the electron pressure, P_e , proton pressure, P_p and neutron pressure, P_n . Combining Eq.(34) with Eq.(35), we can conclude that the total matter energy density, ϵ , increases with increasing B .

The stable configurations of a NS can be obtained from the well-known hydrostatic equilibrium equations of Tolman, Oppenheimer and Volkov (TOV) for the pressure $P(r)$ and the enclosed mass $m(r)$,

$$\begin{aligned} \frac{dP(r)}{dr} &= -\frac{G(m(r) + 4\pi r^3 P(r)/c^2)(\rho + P(r)/c^2)}{r(r - 2Gm(r)/c^2)} \\ \frac{dm(r)}{dr} &= 4\pi \rho r^2, \end{aligned} \quad (36)$$

where G is the gravitational constant, see Ref. 7. For a chosen central value of ρ , the numerical integration of Eq.(23) provides the mass-radius relation. However, we focus on a qualitative analysis of relation of $m(r)$ and B in the context of a magnetar. In Eq.(36), the pressure $P(r)$ is the gravitational collapse pressure, and always be balanced by the total matter pressure, P ; the central density ρ is proportional to the matter energy density ϵ ; the enclosed mass, $m(r)$, increases with the central density ρ when r is given. From the calculations and analysis in this Section, we may expect a more massive stellar mass of a magnetars because the matter energy density, ϵ , increases with B . Also, we propose that magnetars' instability could be associated with the increased gravitational collapse pressure and high chemical potentials of fermions.

As we know, the magnetic effects can give rise to an anisotropy of the total pressure of the system to become anisotropic, e.g., see Ref. 44, 45, 46, 47, 48, 49. In an ideal npe system, the total energy momentum tensor due to both matter and magnetic field is to be given by

$$T^{\mu\nu} = T_m^{\mu\nu} + T_B^{\mu\nu}, \quad (37)$$

where,

$$T_m^{\mu\nu} = \epsilon_m u^\mu u^\nu - P_m (g^{\mu\nu} - u^\mu u^\nu), \quad (38)$$

and

$$T_B^{\mu\nu} = \frac{B^2}{4\pi} (u^\mu u^\nu - \frac{1}{2} g^{\mu\nu}) - \frac{B^\mu B^\nu}{4\pi}. \quad (39)$$

where ϵ_m is the total matter energy density, and P_m is the total matter pressure of the npe system, respectively. The first term in Eq.(39) is equivalent to magnetic pressure, while the second term causes the magnetic tension. Assuming a uniform magnetic field B directed along the z -axis, then we have

$$T_B^{\mu\nu} = \begin{bmatrix} \frac{B^2}{8\pi} & 0 & 0 & 0 \\ 0 & \frac{B^2}{8\pi} & 0 & 0 \\ 0 & 0 & \frac{B^2}{8\pi} & 0 \\ 0 & 0 & 0 & -\frac{B^2}{8\pi} \end{bmatrix}. \quad (40)$$

Due to an excess negative pressure or tension along the direction to the magnetic field, the component of $T_B^{\mu\nu}$ along the field, T_B^{zz} , is negative. Thus, the total pressure in the parallel direction to the magnetic field can be written as

$$P_{\parallel} = P_m - \frac{B^2}{8\pi}, \quad (41)$$

and that perpendicular to the magnetic field, P_{\perp} , is written as

$$P_{\perp} = P_m + \frac{B^2}{8\pi}. \quad (42)$$

From Eqs.(41-42), it's obvious that the total pressure of the system becomes anisotropic. The parallel pressure P_{\parallel} becomes negative, assuming that the magnetic pressure exceeds P_m . However, according to our calculations, when $B^* = 100$,

$P_m \sim 10^{33} - 10^{34}$ dynes cm^{-2} and $\frac{B^2}{8\pi} \sim 10^{29} - 10^{30}$. Hence, in this presentation, we consider that the component of the total energy momentum tensor along the symmetry axis becomes positive, $T^{zz} > 0$, since the total matter pressure increases more rapidly than the magnetic pressure. Accordingly, the total energy momentum tensor is given by

$$T^{\mu\nu} = \begin{bmatrix} \epsilon_m + \frac{B^2}{8\pi} & 0 & 0 & 0 \\ 0 & P_m + \frac{B^2}{8\pi} & 0 & 0 \\ 0 & 0 & P_m + \frac{B^2}{8\pi} & 0 \\ 0 & 0 & 0 & (P_m + \frac{B^2}{8\pi}) - \frac{B^2}{4\pi} \end{bmatrix}. \quad (43)$$

A strong magnetic field can uncover anisotropy, see Ref. 47, 48, due to magnetization pressure, $\mathcal{M}B$, where \mathcal{M} is the magnetization of the system, which is given by

$$\mathcal{M} = -\frac{\partial \epsilon_m}{\partial B}. \quad (44)$$

Therefore, the pressure perpendicular to the magnetic field, P_{\perp} , is actually written as

$$P_{\perp} = P_m + \frac{B^2}{8\pi} - \mathcal{M}B. \quad (45)$$

For a magnetic field $B \ll 10^{20}$ G, the magnetization is opposite to the external field B , i.e., $\mathcal{M} < 0$, and it may happen that $P_{\perp} > P_{\parallel}$. For a magnetic field $B \geq 10^{20}$ G, the opposite occurs in some permeable materials where $\mathcal{M} > 0$ and $P_{\perp} < P_{\parallel}$, this is due to ferromagnetic effects which have quantum origin, as in a gas of degenerate neutrons (see Ref. 47, 48).

However, magnetars considered in the present work universally have typical surface dipole magnetic fields $\sim (10^{14} - 10^{15})$ G and inner field strengths not more than 10^{17} G, under which $B^2/8\pi \gg \mathcal{M}B$, and the effects of AMMs of nucleons on the EOS are ignored. Therefore, we exclude magnetization term in the total pressure. In other words, the exclusion of magnetization term cannot affect the result practically for the present purpose. Our model of magnetized ideal npe gas favors the following relation: $P_{\perp} > P_{\parallel}$, which could lead to the Earth-like oblatening effect.

In the work of Bocquet et al. (see Ref 45), the authors considered an extension of the electromagnetic code developed by Bonazzola et al. (see Ref. 44), and simulated high-magnetized rotating NSs. According to their simulations, the component of the total energy momentum tensor along the symmetry axis is negative, and the combined fluid-magnetic medium can develop a magnetic tension. As a result of this tension, the star displays a pinch across the symmetry axis and assumes a flattened shape (see Ref. 45).

Contrary to the work of Bocquet et al. (1995), we propose that the component of the total energy momentum tensor along the symmetry axis becomes positive,

since the total matter pressure always grows more rapidly than the magnetic pressure. However, a similar effect is expected to occur in our present work, where the magnetic tension along the direction to the magnetic field will be responsible for deforming a magnetar along the magnetic field, and turns the star into a kind of oblate spheroid. Be note that such a deformation in shape might even render a more compact magnetar endowed with canonical strong surface fields $B \sim 10^{14-15}$ G. Also, such a deformed magnetar could have a more massive mass because of the positive contribution of the magnetic field energy to the EOS of the system.

4. Two contrary views on the relationship between P_e and B

As we know, the electron pressure, P_e , as well as the electron Fermi energy $E_F(e)$, is generally believed to decrease with increasing magnetic field strength B (e.g., Ref. 9, 50).

According to statistical physics, the microscopic state number in a 6-dimension phase-space element $dx dy dz dp_x dp_y dp_z$ is $dx dy dz dp_x dp_y dp_z / h^3$. In the Ref. 51, the number of states occupied by completely degenerate relativistic electrons in an unit volume is calculated as follows:

$$\begin{aligned} N_{phase} &= \sum_{p_x} \sum_{p_y} \sum_{p_z} = \frac{1}{h^3} \int_{-\infty}^{\infty} \int_{-\infty}^{\infty} \int_{-\infty}^{\infty} dp_x dp_y dp_z \\ &= \frac{1}{h^3} \int_0^{p_F} dp_z \int_0^{\infty} p_{\perp} dp_{\perp} \int_0^{2\pi} d\Phi = \frac{\pi p_F}{h^3} \int_0^{\infty} dp_{\perp}^2, \end{aligned} \quad (46)$$

where $\Phi = \tan^{-1} p_y / p_x$. Quantization requires $p_{\perp}^2 \rightarrow m^2 c^4 \frac{B}{B_{cr}} 2n$, hence, $\int_0^{\infty} dp_{\perp}^2 \rightarrow \sum_{n=0}^{\infty} \omega_n$, where ω_n is the degeneracy of the n -th Landau level of electrons in relativistic magnetic field, which can be estimated as

$$\begin{aligned} \omega_n &= \frac{1}{h^2} \int_0^{2\pi} d\phi \int_{A < p_{\perp}^2 < B} p_{\perp} dp_{\perp} \\ &= \frac{2\pi (B - A)}{h^2} = \frac{1}{2\pi} \left(\frac{\hbar}{m_e c} \right)^{-2} \frac{B}{B_{cr}}, \end{aligned} \quad (47)$$

where $A = m^2 c^2 \frac{B}{B_{cr}} 2n$, and $B = m^2 c^2 \frac{B}{B_{cr}} 2(n + 1)$ (see Ref. 52)

Be note, the above calculation method was cited from *Statistical Mechanics (1965)* (see Ref. 53). The classical textbook, *Statistical Mechanics (2003)* (see Ref. 54), also gives the expression for the degeneracy of the n -th Landau level of electrons in a relativistic magnetic field,

$$\begin{aligned} \omega_n &= \frac{1}{h^2} \int dp_x dp_y = \frac{1}{h^2} \pi p_{\perp}^2 \Big|_n^{n+1} \\ &= \frac{4\pi m_e \mu_e B}{h^2} = \frac{1}{2\pi} \left(\frac{\hbar}{m_e c} \right)^{-2} \frac{B}{B_{cr}}, \end{aligned} \quad (48)$$

where $\mu_e' = \frac{e\hbar}{2m_e c}$ is the electron magnetic moment. In the momentum interval Δp_z along the direction to the magnetic field, for a non-relativistic electron

gas, the number of possible microstates is given by

$$\frac{eBS}{2\pi\hbar c} \frac{L_z}{2\pi\hbar} \Delta p_z = \frac{eBV}{4\pi^2\hbar^2 c} . \quad (49)$$

(see Ref. 55). For the convenience of calculation, we assume $S = 1 \text{ cm}^2$ and $V = 1 \text{ cm}^3$, and consider the electron spin degeneracy $g_{n0} = 2 - \delta_{n0}$ (when $n = 0$, $g_{00} = 1$; when $n \geq 1$, $g_{n0} = 2$). From **Eq.(49)**, we get the expression for the degeneracy of the n -th Landau level of electrons in a non-relativistic magnetic field,

$$\omega_n = g_{n0} \frac{eB}{2\pi\hbar c} = g_{n0} \frac{4\pi m_e \mu_e B}{h^2} , \quad (50)$$

where the solution of the non-relativistic electron cyclotron motion, $\hbar\omega_B = 2\mu_e B$, is used. Confusingly, the expression for the degeneracy of the n -th Landau level of electrons in a relativistic magnetic field is completely in accordance with that for the corresponding non-relativistic case, if one compare Eq.(47)(or Eq.(48)) with Eq.(50). After careful consideration and analysis, we find that Eq.(47) (or Eq.(48)) is just the expression we are looking for, that leads to an incorrect viewpoint on the electron Fermi energy, as well as the electron pressure, prevailing in the world currently. In our opinion, the expression for ω_n in Eq.(47)(or Eq.(48)) is incorrect, because it's against the viewpoint on the quantization of Landau levels. The essence of the above method (or the incorrect deduction) lies in the assumption that the torus located between the n -th Landau level and the $(n+1)$ -th Landau level in momentum space is ascribed to the $(n+1)$ -th Landau level. Such a factitious assumption is equivalent to allow a continuous momentum (or energy) of an electron moving in the direction perpendicular to the magnetic field, which is obviously contradictory to the quantization of Landau levels in the case of a strong magnetic fields. The concept of Landau level quantization clearly tells us that there is no any microscopic quantum state between $p_{\perp}(n)$ and $p_{\perp}(n+1)$. In a word, the main cause of the popular incorrect viewpoint on $E_F(e)$ is due to a factitious assumption.

In order to depict the quantization of Landau levels truly and accurately, we must introduce the Dirac δ -function $\delta(\frac{p_{\perp}}{m_e c} - [2(n + \sigma + \frac{1}{2})B^*]^{\frac{1}{2}})$ (see Ref. 10, 11). As we know, the eigenvector wave function of the Schrödinger equation (or Dirac equation) can be expanded in an infinite series. In the process of deducing the expressions concerning the quantization of Landau levels, we should firstly give a p_z that changes continuously along the direction to the magnetic field, then solve the relativistic Schrödinger equation (or Dirac equation), finally obtain the maximum Landau level number, n_{max} , by truncating the infinite series when the wave function is limited (see Ref. 55). Logically, give p_z firstly, and then determine the maximum Landau level number n_{max} .

As an alternative way to depict the quantization of Landau Levels of electrons

in strong magnetic fields, we rewrite Eq.(50) as

$$\begin{aligned}\omega_n &= \frac{1}{h^2} g_{n0} \int_0^{2\pi} d\phi \int \delta\left(\frac{p_\perp}{m_e c} - \left[2\left(n + \sigma + \frac{1}{2}\right)B^*\right]^{\frac{1}{2}}\right) p_\perp dp_\perp \\ &= \frac{2\pi}{h^2} g_{n0} \int \delta\left(\frac{p_\perp}{m_e c} - \left[2\left(n + \sigma + \frac{1}{2}\right)B^*\right]^{\frac{1}{2}}\right) p_\perp dp_\perp \quad ,\end{aligned}\quad (51)$$

where $\phi = \arctan p_y/p_x$, and $g_{n0} = 2 - \delta_{n0}$ (when $n = 0$, $g_{00} = 1$; when $n \geq 1$, $g_{n0} = 2$) is the electron spin degeneracy. In the interior of a NS, in the light of the Pauli exclusion principle, the electron number density should be equal to its microscopic state density,

$$\begin{aligned}N_{phase} = n_e &= 2\pi \frac{(m_e c)^3}{h^3} \int_0^{\frac{E_F(e)}{m_e c^2}} d\left(\frac{p_z}{m_e c}\right) \sum_{n=0}^{n_{max}(p_z, \sigma, B^*)} \sum g_{n0} \\ &\int_0^{\frac{E_F(e)}{m_e c^2}} \delta\left(\frac{p_\perp}{m_e c} - \left[2\left(n + \sigma + \frac{1}{2}\right)B^*\right]^{\frac{1}{2}}\right) \frac{p_\perp}{m_e c} d\left(\frac{p_\perp}{m_e c}\right) = N_A \rho Y_e \quad .\end{aligned}\quad (52)$$

In a word, when calculating ω_n and N_{phase} , we must take into account the Dirac δ -function, otherwise, we would reach the wrong conclusion that $E_F(e)$ decreases with the increase in B . Be note, in this letter, we first time propose that the electron pressure P_e increases with increasing B , and the popular point of view on P_e will be confronted with a severe challenge from our calculations

5. Summary Conclusions

In this paper we have derived a general expression for pressure of degenerate and relativistic electrons, which holds approximately when $B \gg B_{cr}$. We conclude that the stronger the magnetic field is, the higher the electron pressure becomes. The high electron pressure could be caused by the electron Fermi energy, which increases with the increase in the magnetic field strength. Given these arguments, the popular point of view on P_e will be confronted with a severe challenge from our calculations.

Also, we have taken into account QED effects on EOSs of *BPS* model, *BBP* model and ideal *npe* gas model, and have discussed an anisotropy of the total pressure of ideal *npe* gas due to strong magnetic fields. Magnetars we have adopted in this work have typical surface dipole fields $B_{dip} \sim (10^{14} - 10^{15})$ G, under which the effects of AMMs of nucleons on the total energy density and the total pressure have not been considered. The main conclusions are as follows: The total matter pressure P increases with magnetic field strength B , because chemical potentials of fermions increase with increasing B , given a matter density ρ ; taking into account of QED effects on the EOS, the total pressure is anisotropic; comparing with a common radio pulsar, a magnetar could be a more compact oblate spheroid-like deformed NS, due to the anisotropic total pressure; an increase in the maximum mass of a magnetar is expected because of the positive contribution of the magnetic field energy to the EOS.

Finally, it is earnestly hoped that our calculations can soon be combined with the latest studies and observations of magnetars, to present a deeper understanding of the nature of superhigh magnetic fields and bursts of magnetars.

Acknowledgments

We thank the anonymous referee for the care in reading the manuscript and for valuable suggestions which help us to improve this paper substantially. This work is supported by Xinjiang Natural Science Foundation No.2013211A053. This work is also supported in part by Chinese National Science Foundation through grants No.11173041, No.11003034 and No.11133001, National Basic Research Program of China grants 973 Programs 2009CB824800 and 2012CB821800, and by a research fund from the Qinglan project of Jiangsu Province.

References

References

1. C. Thompson and R. C. Duncan, *Astrophys. J.* **473**, 322 (1996).
2. R. X. Xu, *Astrophys. J. Lett.* **570**, 65 (2002).
3. R. X. Xu, *Mon. Not. R. Astron. Soc.* **356**, 359 (2005).
4. Y. J. Du, G. J. Qiao, R. X. Xu and J. L. Han, *Mon. Not. R. Astron. Soc.* **399**, 1587 (2009).
5. Q. H. Peng and H. Tong, *Mon. Not. R. Astron. Soc.* **378**, 159 (2007).
6. Q. H. Peng and H. Tong, *Proceedings of the 10th Symposium on Nuclei in the Cosmos Mackinac Island, Michigan, USA, 27 JulyC1 August 2008 POS (NIC X) 189*, (2009), [astro-ph.HE/0911.2066v1].
7. S. L. Shapiro and S. A. Teukolsky, *Black Holes, White Dwarfs, and Neutron Stars*, New York, Wiley-Interscience, (1983).
8. D. G. Yakovlev, A. D. Kaminker, O. Y. Gnedin and P. Haensel, *Phys. Rep.* **354**, 1 (2001).
9. D. Lai and S. L. Shapiro, *Astrophys. J.* **383**, 745 (1991).
10. Z. F. Gao, N. Wang, D. L. Song, J. P. Yuan and C.-K. Chou, *Astrophys. Space Sci.* **334**, 281 (2011).
11. Z. F. Gao, Q. H. Peng, N. Wang and C.-K. Chou, *Astrophys. Space Sci.* **342**, 55 (2012).
12. V. Canuto and J. Ventura, *Fund. Cosmic Phys.*, **2**, 203 (1977).
13. Z. F. Gao, Q. H. Peng, N. Wang, C.-K. Chou and W. S. Huo *Astrophys. Space Sci.* **336**, 427 (2011).
14. J. Ventura, W. Nagel and P. Mészáros, *Astrophys. J. Lett.* **233**, 125 (1979).
15. Z. F. Gao, Q. H. Peng, N. Wang and C.-K. Chou, *Chinese Physics B* **21(5)**, 057109(2012).
16. T. Bulik and M. C. Miller, *Mon. Not. R. Astron. Soc.* **288**, 596 (1997).
17. K. Kohri and S. Yamada, *Phy. Rev. D.* **65**, 043006 (2002), [astro-ph/0102225].
18. Wynn C. G. Ho and D. Lai, *Mon. Not. R. Astron. Soc.* **338**, 233 (2003).
19. L. Kuiper, W. Hermsen and M. Mendež, *Astrophys. J.* **613**, 1173 (2004).
20. S. Molkov, K. Hurley, R. Sunyaev, P. Shtykovsky, M. Revnivtsev and C. Kouveliotou, *Astron. Astrophys.* **433**, L13 (2005).

24 *Authors' Names*

21. S. Mereghetti, D. Götz, I. F. Mirabel and K. Hurley, *Astron. Astrophys.* **433** , L9 (2005).
22. She-Sheng. Xue, *Phys. Rev. D.* **68(1)**, 013004(2003).
23. A. Dupays, C. Rizzo, D. Bakalov and G. F. Bignami, *Europhysics Letters.* **82**, 69002 (2008).
24. D. Mazur and J. S. Heyl, *Mon. Not. R. Astron. Soc.***412**, 1381 (2011).
25. R. Battesti and C. Rizzo, *Rep. Prog. Phys.* **76**, 016401 (2013).
26. D. Götz, S. Mereghetti, A. Tiengo and P. Esposito, *Astron. Astrophys.* **449** , L31(2006).
27. L. Kuiper, W. Hermsen, P. R. den Hartog and W. Collmar, *Astrophys. J.***645** , 556 (2006).
28. P. R. den Hartog, L. Kuiper and W. Hermsen, *Astron. Astrophys.***489**, 263 (2008).
29. M. Lyutikov and F. P. Gavriil, *Mon. Not. R. Astron. Soc.***368**, 690 (2006), [astro-ph/0507557].
30. M. G. Baring and A. K. Harding, *Astrophys. Space Sci.* **308** , 109 (2007).
31. N. Rea, S. Zane, R. Turolla, M. Lyutikov and D. Götz, *Astrophys. J.***686** , 1245 (2008).
32. L. Nobili, R. Turolla and S. Zane, *Mon. Not. R. Astron. Soc.***389** , 989 (2008).
33. M. G. Baring, Z. Wadiasingh and P. L. Gonthier, *Astrophys. J.***733** , 61 (2011).
34. P. L. Gonthier, M. T. Eiles, Z. Wadiasingh, and M. G. Baring, *Astronomical Society of the Pacific Conference Series*, eds. W. Lewandowski, O. Maron and J. Kijak, *Electromagnetic Radiation from Pulsars and Magnetars.***466**, 251 (2012)
35. E. E. Salpeter, *Astrophys. J.* **134**, 669 (1961).
36. G. Baym, C. Pethick and P. Sutherland, *Astrophys. J.* **170**, 299 (1971).
37. I. Fushiki, E. H. Gudmundsson and C. J. Pethick, *Astrophys. J.* **342**, 958 (1989).
38. P. Haensel, J. L. Zdunik and J. Dobaczewski, *Astron. Astrophys.* **222**, 353 (1989).
39. A. H. Wapstra and K. Bos, *Atomic Data Nucl. Data Tables.* **19** , 175 (1977).
40. A. H. Wapstra and K. Bos, *Atomic Data Nucl. Data Tables.* **17** , 474 (1976).
41. G. Baym, H. A. Bethe and C. J. Pethick, *Nuclear Phys. A.* **175**, 225 (1971).
42. V. Canuto, *Ann. Rev. Astron. Astrophys.* **12**, 167 (1974).
43. S. Chakrabarty, D. Bandyopadhyay, and S. Pal, *Phy. Rev. Lett.* **78**, 75 (1997).
44. S. Bonazzola, E. Gourgoulhon, M. Salgado and J. A. Marck, *Astron. Astrophys.* **278**, 421 (1993).
45. M. Bocquet, S. Bonazzola, E. Gourgoulhon and J. Novak, *Astron. Astrophys.* **301**, 757 (1995).
46. V.R. Khalilov, *Phys. Rev. D .* **65(5)**, 056001 (2002).
47. A. Pérez Martínez, H. Pérez. Rojas and H. J. Mosquera Cuesta, *Eur. Phys. J. C* **29**,111 (2003),[astro-ph/0303213].
48. A. Pérez Martínez, H. Pérez. Rojas and H. J. Mosquera Cuesta, *Int.J. Mod. Phys. D.***17**, 210 (2008).
49. L. Paulucci, E. J. Ferrer, V. de La Incera and J. E. Horvath, *Phys. Rev. D.* **83(4)**, 043009 (2011).
50. D. Lai, *Reviews of Modern Physics*, **73**, 629 (2001).
51. V. Canuto and H.Y. Chiu, *Phys. Rev.* **173**, 1210 (1968).
52. V. Canuto and H.Y. Chiu, *Space Sci. Rev.*, **12**, 3 (1971).
53. R. Kubo, *Statistics Mechanics* , (Amsterdam: North-Holland Publishing Co. 1965), pp. 278–280.
54. R. K. Pathria, *Statistics Mechanics, 2nd*, (Singapore: Isevier. 2003), p. 280.
55. L. D. Landau and E. M. Lifshitz, *Quantum Mechanics*, ed. W. H. Freeman, (Pergamon Press, New York, 1965), pp. 459-460.